Polariton Localization and Dispersion Properties of Disordered Quantum Emitters in Multimode Microcavities

Georg Engelhardt[1,2,3] and Jianshu Cao[4,*]

[1]Shenzhen Institute for Quantum Science and Engineering, Southern University of Science and Technology, Shenzhen 518055, China

[2]International Quantum Academy, Shenzhen 518048, China

[3]Guangdong Provincial Key Laboratory of Quantum Science and Engineering, Southern University of Science and Technology, Shenzhen 518055, China

[4]Department of Chemistry, Massachusetts Institute of Technology, 77 Massachusetts Avenue, Cambridge, Massachusetts 02139, USA

(Received 16 August 2022; accepted 7 April 2023; published 24 May 2023)

Experiments have demonstrated that the strong light-matter coupling in polaritonic microcavities significantly enhances transport. Motivated by these experiments, we have solved the disordered multimode Tavis-Cummings model in the thermodynamic limit and used this solution to analyze its dispersion and localization properties. The solution implies that wave-vector-resolved spectroscopic quantities can be described by single-mode models, but spatially resolved quantities require the multimode solution. Nondiagonal elements of the Green's function decay exponentially with distance, which defines the coherence length. The coherent length is strongly correlated with the photon weight and exhibits inverse scaling with respect to the Rabi frequency and an unusual dependence on disorder. For energies away from the average molecular energy E_{M} and above the confinement energy E_C, the coherence length rapidly diverges such that it exceeds the photon resonance wavelength λ_0. The rapid divergence allows us to differentiate the localized and delocalized regimes and identify the transition from diffusive to ballistic transport.

DOI: 10.1103/PhysRevLett.130.213602

Introduction.—The spatial confinement of the light field in microcavities gives rise to dispersive polaritons with outstanding spectroscopic properties [1] and establishes an alternative channel for charge and energy transport different from the short-range hopping. Recent experimental measurements of microcavities have found that transport can be enhanced by orders of magnitude [2–7]. A thorough description is challenging because of the large number of light modes in the cavity and the energetic, spatial, and orientational disorder.

Many theoretical models describe the light field by a single cavity mode, which is coupled to a macroscopic number of quantum emitters [8–27]. Recent investigations have predicted an intriguing turnover of the transport, relaxation, and the linewidth as a function of disorder [8,9]. However, due to the all-to-all coupling structure in single-mode models, excitons can travel instantaneously between distant emitters and thus exceed the speed of light, potentially leading to an unphysical prediction for the transport efficiency.

Since the photonic dispersion relation ensures the speed of light, the light fields should be described as a continuum of cavity modes. For example, the impact of disorder on polaritons was investigated perturbatively [28–31]. Exact diagonalization and integration [32,33], mean-field based approaches [34–37], Monte-Carlo methods [38], and density-functional theory [39] have been used to numerically investigate multimode models. Yet, a fully microscopic and analytical solution of the light-matter dynamics for disordered quantum emitters is still lacking.

In this Letter, we analytically and numerically solve the multimode disordered Tavis-Cumming model nonperturbatively. Our closed-form solution predicts a finite coherence length for all polariton energies. Away from the average molecular energy E_{M}, the coherence length rapidly diverges and exceeds by far the typical length of realistic microcavities. This defines two transport regimes in the energy spectrum: one regime of strongly localized polaritons, where transport is diffusive, and one regime of delocalized polaritons, where the large coherence length can support ballistic transport. The coherence length exhibits a turnover as a function of disorder, which has no analog in the Anderson localization [40–42], but is reminiscent of noise-assisted transport [43,44].

Multimode disordered Tavis-Cummings model.—As shown in Figs. 1(a) and 1(b), we consider a one-dimensional microcavity of length L which contains N quantum emitters representing atoms, molecules, NV centers, or particle-hole pairs in semiconductors. For concreteness, we focus on molecules in the following. We adopt a multimode disordered Tavis-Cummings model, whose Hamiltonian is given as $\hat{H} = \hat{H}_{\mathrm{M}} + \hat{H}_{\mathrm{L}} + \hat{H}_{\mathrm{LM}}$, where

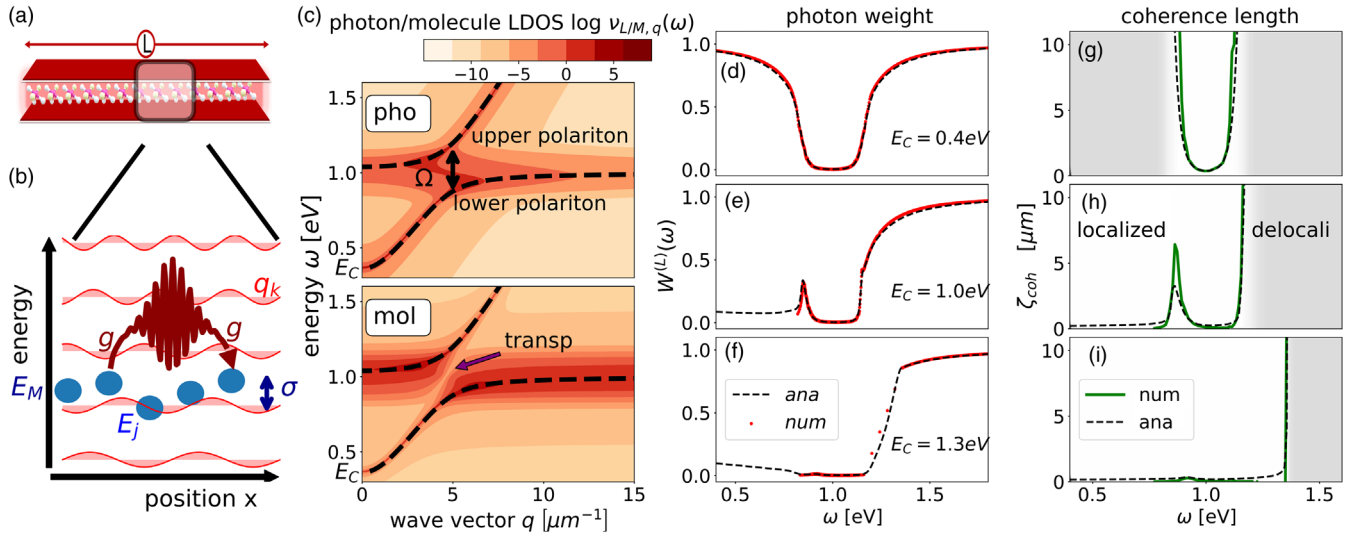

FIG. 1. (a) One-dimensional microcavity of length L containing N molecules. (b) Sketch of the energy configuration of the cavity modes (red sine functions) and the molecules (blue circles, E_j distributed around E_M with Gaussian width σ). The molecules are coupled with strength $g_{j,k}$ to the photonic modes, such that excitations can be transported via photons. (c) Wave-vector-resolved photon and molecule LDOSs for $E_C = 0.4$ eV. (d),(e),(f) Average photon weight of the polaritons as a function of energy for $E_C = 0.4$, 1.0, 1.3 eV. (g),(h),(i) Coherence length of the polaritons for the same E_C values as in (d),(e),(f). Overall parameters are $L = 125$ μm, $N = 5000$, $E_M = 1$, $\sigma = 0.05$, and $g\sqrt{\rho} = 0.14$ eV. The photonic cutoff energy is $\omega_{\text{cutoff}} = 50$ eV, such that 5000 photonic modes are included in the simulations.

$$\hat{H}_M = \sum_{j=1}^{N} E_j \hat{B}_j^\dagger \hat{B}_j, \qquad \hat{H}_L = \sum_k \omega_k \hat{a}_k^\dagger \hat{a}_k,$$
$$\hat{H}_{LM} = \sum_{j=1}^{N} \sum_k g_{j,\kappa} \hat{B}_j^\dagger \hat{a}_k + \text{H.c.} \tag{1}$$

The molecules j are described by bosonic operators $\hat{B}_j$. Here, the excitation energies E_j are distributed according to a Gaussian function $P(E) = (1/\sqrt{\pi}\sigma)e^{-(E-E_M)^2/(2\sigma^2)}$, with center E_M and disorder width σ. Yet, our findings also hold for arbitrary disorder distributions. The light field is quantized by the photonic operators $\hat{a}_k$ labeled by k. The photonic dispersion relation is $\omega_k = \sqrt{c^2 q_k^2 + E_C^2}$, where c is the speed of light, q_k is the wave vector (specified below), and E_C is the confinement energy depending on the geometry of the microcavity. As the total excitation number $\hat{n} = \sum_j \hat{B}_j^\dagger \hat{B}_j + \sum_k \hat{a}_k^\dagger \hat{a}_k$ is conserved, we can restrict our analysis to the single-excitation manifold. The light-matter interaction in Eq. (1) is given by $g_{j,k} = g_k \varphi_k(r_j)$, where $r_j = jL/N$ is the position of molecule j, g_k is the wave vector dependent light-matter interaction, and $\varphi_k(r)$ are the photonic mode functions in one-dimensional space. We restrict the current investigation to energetic disorder, while spatial and orientational disorder will be considered elsewhere later.

For the numerical calculations we use an open boundary condition, such that the photonic modes are $\varphi_k(r) = \sin(q_k r)/\sqrt{L/2}$ for the wave vectors $q_k = \pi k/L$ with integer $k > 0$ [45]. In the analytical calculation, we assume a periodic boundary condition such that the photonic modes are $\varphi_k(r) = \exp(iq_k r)/\sqrt{L}$, where $q_k = 2\pi k/L$ with integer k. We note that in the $L \to \infty$ limit, the boundary condition has a negligible effect.

Analytical solution.—The Heisenberg equations of $\hat{B}_j$ and $\hat{a}_k$ are transformed into the Laplace space defined by $\hat{f}(z) = \int_0^\infty dt e^{-zt} \hat{f}(t)$ for arbitrary operators $\hat{f}(t)$. We find that the coupling between different cavity modes k_1, k_2 scales as $\hat{a}_{k_1}(z) \propto \rho N^{-1/2} \hat{a}_{k_2}(z)$ and thus vanishes in the thermodynamic limit $N, L \to \infty$ with constant density $\rho = N/L$ [45]. In other words, one can treat the system as a superposition of uncoupled single-mode systems, which have been investigated in detail in Refs. [9,46,47]. The solution of the Heisenberg operators in this limit is

$$\hat{a}_k(z) = \frac{\hat{a}_k^{(0)}}{z + i\omega_k(z)} - i\sum_j \frac{g_{j,k}\hat{B}_j^{(0)}}{[z + i\omega_k(z)](z + iE_j)},$$
$$\hat{B}_j(z) = \frac{\hat{B}_j^{(0)}}{z + iE_j} - i\sum_k \frac{g_{j,k}\hat{a}_k^{(0)}}{(z + iE_j)[z + i\omega_k(z)]}$$
$$- \sum_k \sum_{j_1} \frac{g_{j,k} g_{j_1,k}^* \hat{B}_{j_1}^{(0)}}{(z + iE_j)[z + i\omega_k(z)](z + iE_{j_1})}, \tag{2}$$

where $\hat{a}_k^{(0)}$ and $\hat{B}_j^{(0)}$ denote the initial conditions of the time evolution. We have defined the renormalized photon energy by

$$\omega_k(z) = \omega_k - i\sum_j \frac{|g_{j,k}|^2}{z + iE_j} \to \omega_k + g_k^2 \rho \Gamma(z), \quad (3)$$

where the z dependence reflects a retardation effect. We have expressed the disorder average in terms of the density ρ and the disorder-averaged Green's function of the unperturbed molecules $\Gamma(z) = -i\int dE[P(E)/(z+iE)]$. Using Eq. (2), we can construct arbitrary retarded Green's functions such as $G^{(\mathrm{L})}_{k,k'}(z) \equiv -i\langle[\hat{a}_k(z), \hat{a}^{(0)\dagger}_{k'}]\rangle$ or $G^{(\mathrm{M})}_{j,j'}(z) \equiv -i\langle[\hat{B}_j(z), \hat{B}^{(0)\dagger}_{j'}]\rangle$. Performing the disorder average, the Green's function for $N, L \to \infty$ reads as

$$G^{(\mathrm{L})}_{k,k'}(z) = -i\frac{\delta_{k,k'}}{z + i\omega_k(z)},$$
$$G^{(\mathrm{M})}_{j,j'}(z) = \Gamma(z)\delta_{j,j'} - i\sum_k \frac{g_{j,k}g^*_{j_1,k}}{z + i\omega_k(z)}\rho\Gamma(z)^2. \quad (4)$$

These Green's functions are equivalent to the single-mode system when the sum over k is neglected. The simple superposition of all k modes reflects the mode decoupling in the thermodynamic limit, for which the matter system becomes homogeneous in a statistical sense.

Spectroscopy.—The wave-vector-resolved photon and molecule local density of states (LDOSs) are given as $\nu_{X,k}(\omega) \equiv -\lim_{\delta\downarrow 0}(1/\pi)\mathrm{Im}G^{(X)}_{k,k}(-i\omega+\delta)$ with $X = \mathrm{L}$ and $X = \mathrm{M}$, respectively, and can be measured spectroscopically [9].

In Fig. 1(c), we investigate the LDOSs for $E_C = 0.4$ eV. The LDOSs for $E_C = 1.0$ and $E_C = 1.3$ eV can be found in the Supplemental Material [45]. The dashed lines depict the lower and upper polaritons for a vanishing disorder $\sigma = 0$. Close to $\omega_k = E_\mathrm{M}$, where both dispersions would cross for $g = 0$, the lower and upper polaritons exhibit a Rabi splitting of $\Omega \approx 2g\sqrt{\rho}$. The photon and molecule LDOSs closely follow the photonic dispersion curves of the disorder-free systems (dashed). The photon LDOS accumulates close to the photon dispersion ω_k, but also around E_M close to the polariton anticrossing, where light and matter are strongly mixed. The molecule LDOS accumulates around E_M, where it resembles the original disorder distribution. Along ω_k and away from E_M, the molecule LDOS is one order of magnitude smaller than the photon LDOS. Because of level repulsion, the molecule LDOS is suppressed for energies ω_k at the anticrossing (purple arrow), which resembles the electromagnetically induced transparency and related effects [9,48–50]. As each photon mode interacts with a disordered ensemble, the level repulsion is smeared out in the photon LDOS.

The photon and molecule weights of a specific eigenstate $|\alpha\rangle$ with energy ω is given as $W^{(X)}(\omega) \equiv \langle\alpha|\hat{P}^{(X)}|\alpha\rangle = \sum_k \nu_{X,k}(\omega)/\nu(\omega)$, where $\nu(\omega) = \sum_{X=\mathrm{L,M};k}\nu_{X,k}(\omega)$, and $\hat{P}^{(X)}$ is the photon (molecule) projection operator. The

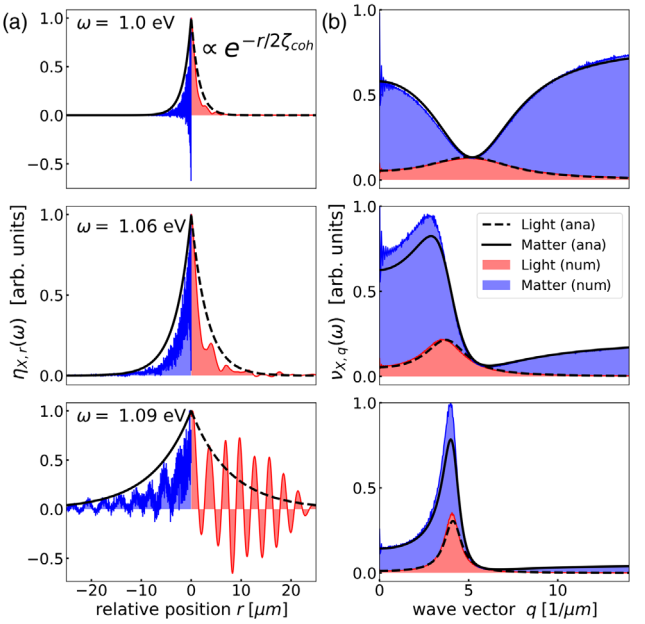

FIG. 2. (a) Imaginary part of the Green's function as a function of the relative position coordinate $r = r_j - r_{j'}$ as defined in Eq. (5). The results are shown in red (photon contribution, $r > 0$) and blue (molecule contribution, $r < 0$). The black lines depict the amplitude decay predicted by the coherence length in Eq. (7). (b) Imaginary part of the Green's function as a function of wave vector (i.e., the LDOS). The solid and dashed black lines depict the analytical predictions using Eq. (4). Parameters are the same as in Fig. 1(d). Each Green's function has been averaged over an interval of width $\delta = 0.005$ [eV].

numerical calculation in Figs. 1(d)–1(f) verifies the analytical solution for various E_C. (i) For $E_C = 0.4$ eV $< E_\mathrm{M}$, the photon weight vanishes around the resonance condition $\omega \approx 1$ eV, as the molecules by far outnumber the photon modes in this energy region. The photon weight increases monotonically with increasing distance from the resonance condition. (ii) For $E_C = 1.0$ eV $= E_\mathrm{M}$, the photon weight does not monotonically increase with distance from E_M. The peak around $\omega \approx 0.9$ eV is a consequence of the polariton formation, causing the light field to be pushed down energetically. (iii) For $E_C = 1.3$ eV $> E_\mathrm{M}$, light and matter are energetically separated such that the mutual influence is rather weak. Motivated by Ref. [32], we define dark (bright) states as eigenstates with a photonic weight $W^{(\mathrm{L})} < 10\%$ ($W^{(\mathrm{L})} > 10\%$), which accumulate in the dip of the photon weight in Fig. 1(d).

Polariton localization.—Figure 2(a) depicts the imaginary part of the Green's function in position space,

$$\eta_{X,r}(\omega) \equiv -\lim_{\delta\downarrow 0}\frac{1}{\pi}\mathrm{Im}G^{(X)}_{j,j'}(-i\omega+\delta) \propto e^{-\frac{r}{2\zeta_\mathrm{coh}}}, \quad (5)$$

where $r = |r_j - r_{j'}|$, for $E_C = 0.4$ eV and three different energies ω. In this definition we have used the translational

invariance of the Green's function in the $N \to \infty$ limit. The photon (molecule) Green's function is depicted for $r > 0$ ($r < 0$). Clearly, the amplitude of the Green's function shows an exponential decay with increasing r, where the coherence length ζ_{coh} depends on energy.

Figure 2(b) depicts the imaginary part of the Green's function in wave vector space, i.e., $\nu_{X,k}(\omega)$ for $X = \mathrm{L}, \mathrm{M}$. Overall, we observe that the widths of the Green's functions in position and wave vector space are related by the Heisenberg uncertainty principle. In contrast to the photon contribution, which converges to zero for large wave vectors q, the molecule Green's function converges to a finite value. This is reflected by strong spatial fluctuations of the molecule Green's function in position space in Fig. 2(a), which are absent in the photon Green's function.

From Eq. (4) we can determine the coherence length ζ_{coh} using functional analysis, which characterizes the localization of the polaritons [45,51]: In the $L \to \infty$ limit, we find

$$\eta_{\mathrm{L},r}(\omega) \propto G^{(\mathrm{L})}_{j,j'}(-i\omega) = \int dq\, G_q(\omega) e^{iqr}, \tag{6}$$

where $r = |r_j - r_{j'}| \neq 0$ and $G_q(\omega) = (-i)/[-i\omega + i\omega_{qL/2\pi}(-i\omega)]$. Specifically, the Green's function decays as $\propto e^{-\alpha r}$, where α is the largest value such that $G_{q-i\alpha'}$ is analytic for all $|\alpha'| < \alpha$. G_q has two types of non-analyticities, namely the roots of the denominator and the branch cuts along the imaginary axis $\pm q \in [iE_C/c, i\infty]$ due to the root in ω_k. As explained later, the branch cut has minor influence on $\eta_{X,r}$, such that the coherence length is effectively determined by the root of G_q, i.e.,

$$\zeta^{-1}_{\mathrm{coh}} = \frac{2}{c}\mathrm{Im}\sqrt{[\omega - g^2\rho\Gamma(-i\omega)]^2 - E_C^2}, \tag{7}$$

where $g_k = g$ is assumed for simplicity. Interestingly, the coherence length depends via the product $g\sqrt{\rho} = \Omega/2$ (i.e., the Rabi frequency) on the light-matter coupling g.

In Figs. 1(g)–1(i), we compare the analytical expression for ζ_{coh} with the numerical evaluation [45], which confirms the validity of the analytical solution. For large energies ω, we observe that the coherence length diverges. For realistic parameters and energies $\omega \approx E_{\mathrm{M}}$, the branch cuts starting at $\pm i(E_C/c)$ have a minor influence on the coherence length, as for a large E_C, $2c/E_C$ is significantly smaller than ζ_{coh}, while for small E_C, the influence of the branch cut in the Fourier transformation in Eq. (6) is negligible and the Green's function is still mainly determined by the pole of the Green's function [45].

Analysis.—In Fig. 1 we demonstrate a correlation between the photon weight and the coherence length. As the interaction between the molecules is mediated via photons, the coherence length increases when photons can travel further without being scattered by molecules. The relation of coherence length and photon scattering can be understood by expanding the Green's function in orders of g, where destructive interference of distinct photon scattering paths decrease the coherence length for increasing g [45]. A low scattering probability is reflected by a large photon weight in the Green's function. The coherence length of the Green's function can thus be identified with the absorption length for light traveling along the extended direction of the cavity according to Beer's absorption law [45]. Dark states have a detrimental impact on the coherence length. In general, we find a clear relation of dark states with a localized Green's function, and bright states with a delocalized Green's function. The localized (delocalized) regimes are thereby described by $\zeta_{\mathrm{coh}} < \lambda_0$ ($\zeta_{\mathrm{coh}} > \lambda_0$), where $\lambda_0 = hc/E_{\mathrm{M}}$ is the resonance wavelength of the molecular excitations.

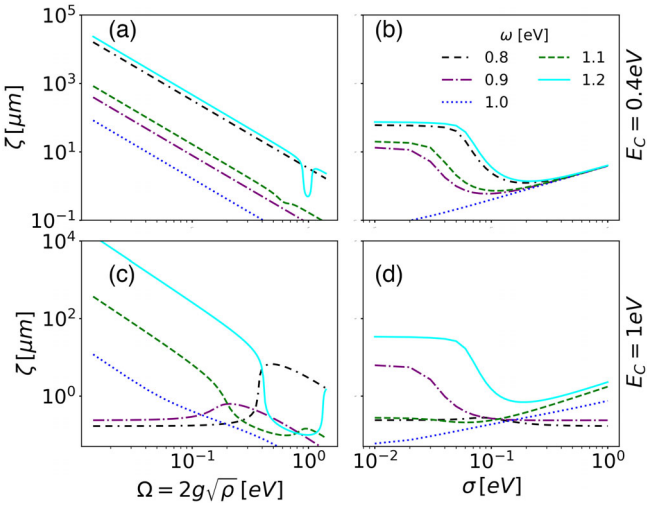

FIG. 3. Coherence length as a function of Rabi splitting [(a),(c)] and disorder [(b),(d)]. Parameters are the same as in Fig. 1.

In Fig. 3, we analyze the coherence length ζ_{coh} as a function of $\Omega = 2g\sqrt{\rho}$ and σ for $E_C = 0.4$ and $E_C = 1.0$ eV. In Fig. 3(a) for small Ω, we observe a clear linear dependence with slope -2 for all energies ω. This can be explained by photon scattering, which consists of absorption ($\propto g\rho$) and reemission ($\propto g$). Interestingly, the coherence length for $\omega = 1.2$ eV exhibits a dip for large Ω, as the matter LDOS is strongly deformed and accumulates around $\omega = 1.2$ eV, causing enhanced photon scattering.

The observations in Fig. 3(c) for $E_C = 1.0$ eV and large $\omega = 1.0, 1.1, 1.2$ eV are qualitatively similar to panel (a). The coherence length behaves very differently for small ω, where the photonic modes are absent for $g = 0$ as $\omega_k > E_C$. As for these energies eigenstates can be only formed with non-resonant photon modes, the coherence length for small Ω is very small and almost independent of Ω [45]. Interestingly, the coherence length increases over more than 1 order of magnitude for $\Omega \approx 0.3$ and $\omega = 0.8$ eV

because of the peak in the photon weight for small energies $\omega \approx 0.8$ eV in Fig. 1(e).

Analyzing the coherence length as a function of disorder in Fig. 3(b), we observe a turnover as a function of σ. This is in contrast to the Anderson localization, where the coherence length monotonically decreases with disorder. Recent work has revealed a turnover of the steady-state flux as a function of disorder in the single-mode Tavis-Cummings model [8,9,15], which can be explained by the overlap of the photon LDOS and the molecule energy disorder distribution $P(E)$ [9]. This interpretation can also be employed here. For small σ, the disorder distribution is strongly centered around E_{M}. With increasing σ, the disorder distribution increases for $\omega \neq E_{\mathrm{M}}$, such that more molecules can resonantly scatter the photons with energy ω, which reduces the coherence length. For a large disorder, the molecule energies spread over a large energy regime, such that there are only few molecules in resonance with the photon modes close to ω, which enhances the coherence length. As the Gauss distribution becomes very flat close to the center for large σ, the coherence length becomes independent of ω for large σ. For $\omega = 1.0$ eV, we do not observe a turnover, as the disorder distribution $P(\omega \approx E_{\mathrm{M}})$ decreases monotonically for increasing σ. The turnovers can be also observed for $E_C = 1.0$ eV in Fig. 3(d) for large $\omega = 1.1, 1.2$ eV, while overall the dependence on σ is more complicated because of the significant influence of the square root dispersion relation of ω_k close to $q = 0$.

Conclusions.—We have analytically and numerically solved the multimode disordered Tavis-Cummings model and predict its dispersion and localization properties. (i) The analytical solution is built on the mode decoupling and statistical self-averaging and is exact in the thermodynamic limit. Based on the solution, wave-vector-resolved properties such as broadened spectral line shape and dispersion can be predicted effectively within the single-mode treatment, whereas spatial-dependent properties such as transport and coherence length involve a wave vector summation and thus require the multimode formalism. (ii) A coherence length is introduced to characterize the finite size of the eigenstates as a function of the excitation energy and shows transitions from localized states around the molecular energy (E_{M}) to delocalized states away from E_{M}. These transitions are strongly correlated with the photon weight and define a ballistic and a localized transport regime. (iii) Intriguingly, the coherence length is inversely proportional to the square of the Rabi frequency and can exhibit a turnover as a function of disorder. (iv) Both the dispersion and coherence length depend strongly on the cavity confinement energy E_C: the number of available resonant photon modes and thus the light-matter coupling regime increase as the cavity changes from blueshifted ($E_C > E_{\mathrm{M}}$), resonance ($E_C = E_{\mathrm{M}}$), to redshifted ($E_C < E_{\mathrm{M}}$). The current investigation focuses on the one-dimensional system with energetic disorder, while higher-dimensional systems with spatial and orientational disorder will be considered elsewhere.

The coherence length crucially depends on the light-matter coupling and the disorder. For example, it can be enhanced by more than one order of magnitude with a slight increase of the light-matter interaction [cf. Fig. 3(c)]. Moreover, it can exhibit a turnover as a function of disorder, which contrasts the monotonically decreasing coherence length known from the Anderson localization, but is reminiscent of noise-assisted quantum transport [52–55]. Arising from the overlap of the light LDOS and the disorder distribution, this turnover is induced by the same mechanism as the transport turnover previously predicted in the single-mode disordered Tavis-Cummings model [9]. Experimentally, this turnover can be investigated using a mixture of two molecular ensembles as in [18].

Noteworthy, the experiment in Ref. [7] has identified a transition from diffusive transport for small photonic weight to ballistic transport for large photonic weight. This observation is in perfect agreement with our analytical calculation, which predicts localized (i.e., diffusive) and delocalized (i.e., ballistic) eigenstates and a sharp transition as a function of excitation energy, as shown in Fig. 1. These findings reveal that the photonic weight explains the enhanced transport efficiency. In general, dark states with low photon weight correspond to localized states, while bright states with high photon weight correspond to delocalized states.

The experiment in Ref. [38] indicates that phonon-assisted coupling of diffusive eigenstates and ballistic eigenstates helps to overcome the localization. Extending our current model in Eq. (1) to incorporate phonon modes will quantitatively demonstrate this mechanism. Moreover, as experimentally shown in [56], the detrimental impact of the cavity quality on transport properties can be modeled by a complex dispersion relation $\omega_k \to \omega_k - i\kappa$ with $\kappa > 0$. This will result in a complex energy shift $\omega \to \omega + i\kappa$ in the coherence length in Eq. (7), leading to a suppression of transport. These and other experimental implications will be studied in future works.

G. E. gratefully acknowledges financial support from the Guangdong Provincial Key Laboratory of Quantum Science and Engineering (Grant No. 2019B121203002); J. C. acknowledges support from the NSF (Grants No. CHE1800301 and No. CHE1836913), the MIT sloan fund, and the Maria Curie FRIAS COFUND Fellowship Programme (FCFP) during his sabbatical in Germany.

*jianshu@mit.edu

[1] F. J. Garcia-Vidal, C. Ciuti, and T. W. Ebbesen, Manipulating matter by strong coupling to vacuum fields, Science **373**, 0336 (2021).

[2] G. Lerario, D. Ballarini, A. Fieramosca, A. Cannavale, A. Genco, F. Mangione, S. Gambino, L. Dominici, M. De

Giorgi, G. Gigli, and D. Sanvitto, High-speed flow of interacting organic polaritons, Light Sci. Appl. **6**, e16212 (2017).

[3] E. Orgiu, J. George, J. A. Hutchison, E. Devaux, J. F. Dayen, B. Doudin, F. Stellacci, C. Genet, J. Schachenmayer, C. Genes, G. Pupillo, P. Samorì, and T. W. Ebbesen, Conductivity in organic semiconductors hybridized with the vacuum field, Nat. Mater. **14**, 1123 (2015).

[4] G. G. Rozenman, K. Akulov, A. Golombek, and T. Schwartz, Long-range transport of organic exciton-polaritons revealed by ultrafast microscopy, ACS Photonics **5**, 105 (2018).

[5] S. Hou, M. Khatoniar, K. Ding, Y. Qu, A. Napolov, V. M. Menon, and S. R. Forrest, Ultralong-range energy transport in a disordered organic semiconductor at room temperature via coherent exciton-polariton propagation, Adv. Mater. **32**, 2002127 (2020).

[6] N. Krainova, A. J. Grede, D. Tsokkou, N. Banerji, and N. C. Giebink, Polaron Photoconductivity in the Weak and Strong Light-Matter Coupling Regime, Phys. Rev. Lett. **124**, 177401 (2020).

[7] M. Balasubrahmaniyam, A. Simkhovich, A. Golombek, G. Sandik, G. Ankonina, and T. Schwartz, From enhanced diffusion to ultrafast ballistic motion of hybrid light-matter excitations, Nat. Mater. **22**, 338 (2023).

[8] N. C. Chávez, F. Mattiotti, J. A. Méndez-Bermúdez, F. Borgonovi, and G. L. Celardo, Disorder-Enhanced and Disorder-Independent Transport with Long-Range Hopping: Application to Molecular Chains in Optical Cavities, Phys. Rev. Lett. **126**, 153201 (2021).

[9] G. Engelhardt and J. Cao, Unusual dynamical properties of disordered polaritons in microcavities, Phys. Rev. B **105**, 064205 (2022).

[10] J. Feist and F. J. Garcia-Vidal, Extraordinary Exciton Conductance Induced by Strong Coupling, Phys. Rev. Lett. **114**, 196402 (2015).

[11] C. Sommer, M. Reitz, F. Mineo, and C. Genes, Molecular polaritonics in dense mesoscopic disordered ensembles, Phys. Rev. Res. **3**, 033141 (2021).

[12] F. C. Spano, Optical microcavities enhance the exciton coherence length and eliminate vibronic coupling in J-aggregates, J. Chem. Phys. **142**, 184707 (2015).

[13] N. Shammah, N. Lambert, F. Nori, and S. De Liberato, Superradiance with local phase-breaking effects, Phys. Rev. A **96**, 023863 (2017).

[14] T. Botzung, D. Hagenmüller, S. Schütz, J. Dubail, G. Pupillo, and J. Schachenmayer, Dark state semilocalization of quantum emitters in a cavity, Phys. Rev. B **102**, 144202 (2020).

[15] J. Dubail, T. Botzung, J. Schachenmayer, G. Pupillo, and D. Hagenmüller, Large random arrowhead matrices: Multifractality, semilocalization, and protected transport in disordered quantum spins coupled to a cavity, Phys. Rev. A **105**, 023714 (2022).

[16] Q. Zhang and K. Zhang, Collective effects of organic molecules based on the Holstein-Tavis-Cummings model, J. Phys. B **54**, 145101 (2021).

[17] T. Gera and K. L. Sebastian, Exact results for the Tavis-Cummings and Hückel Hamiltonians with diagonal disorder, J. Phys. Chem. A **126**, 5449 (2022).

[18] B. Cohn, S. Sufrin, A. Basu, and L. Chuntonov, Vibrational polaritons in disordered molecular ensembles, J. Phys. Chem. Lett. **13**, 8369 (2022).

[19] F. Herrera and F. C. Spano, Cavity-Controlled Chemistry in Molecular Ensembles, Phys. Rev. Lett. **116**, 238301 (2016).

[20] R. Houdré, R. P. Stanley, and M. Ilegems, Vacuum-field Rabi splitting in the presence of inhomogeneous broadening: Resolution of a homogeneous linewidth in an inhomogeneously broadened system, Phys. Rev. A **53**, 2711 (1996).

[21] B. Xiang, R. F. Ribeiro, L. Chen, J. Wang, M. Du, J. Yuen-Zhou, and W. Xiong, State-selective polariton to dark state relaxation dynamics, J. Phys. Chem. A **123**, 5918 (2019).

[22] M. Reitz, F. Mineo, and C. Genes, Energy transfer and correlations in cavity-embedded donor-acceptor configurations, Sci. Rep. **8**, 9050 (2018).

[23] C. Schäfer, M. Ruggenthaler, H. Appel, and A. Rubio, Modification of excitation and charge transfer in cavity quantum-electrodynamical chemistry, Proc. Natl. Acad. Sci. U.S.A. **116**, 4883 (2019).

[24] J. Cao, Generalized resonance energy transfer theory: Applications to vibrational energy flow in optical cavities, J. Phys. Chem. Lett. **13**, 10943 (2022).

[25] B. Cui and A. Nitzan, Collective response in light-matter interactions: The interplay between strong coupling and local dynamics, J. Chem. Phys. **157**, 114108 (2022).

[26] D. Finkelstein-Shapiro, P.-A. Mante, S. Balci, D. Zigmantas, and T. Pullerits, Non-Hermitian Hamiltonians for linear and nonlinear optical response: A model for plexcitons, J. Chem. Phys. **158**, 104104 (2023).

[27] Z. Zhang, X. Nie, D. Lei, and S. Mukamel, Multidimensional Coherent Spectroscopy of Molecular Polaritons: Langevin Approach, Phys. Rev. Lett. **130**, 103001 (2023).

[28] F. M. Izrailev, S. Ruffo, and L. Tessieri, Classical representation of the one-dimensional Anderson model, J. Phys. A **31**, 5263 (1998).

[29] V. M. Agranovich, M. Litinskaia, and D. G. Lidzey, Cavity polaritons in microcavities containing disordered organic semiconductors, Phys. Rev. B **67**, 085311 (2003).

[30] M. Litinskaya and P. Reineker, Loss of coherence of exciton polaritons in inhomogeneous organic microcavities, Phys. Rev. B **74**, 165320 (2006).

[31] M. Litinskaya, P. Reineker, and V. Agranovich, Fast polariton relaxation in strongly coupled organic microcavities, J. Lumin. **110**, 364 (2004).

[32] R. F. Ribeiro, Multimode polariton effects on molecular energy transport and spectral fluctuations, Commun. Chem. **5**, 48 (2022).

[33] T. F. Allard and G. Weick, Disorder-enhanced transport in a chain of lossy dipoles strongly coupled to cavity photons, Phys. Rev. B **106**, 245424 (2022).

[34] J. Patton, V. Norman, R. Scalettar, and M. Radulaski, All-photonic quantum simulators with spectrally disordered emitters, arXiv:2112.15469.

[35] J. A. Ćwik, S. Reja, P. B. Littlewood, and J. Keeling, Polariton condensation with saturable molecules dressed by vibrational modes, Europhys. Lett. **105**, 47009 (2014).

[36] A. Strashko, P. Kirton, and J. Keeling, Organic Polariton Lasing and the Weak to Strong Coupling Crossover, Phys. Rev. Lett. **121**, 193601 (2018).

[37] I. Sokolovskii, R. H. Tichauer, J. Feist, and G. Groenhof, Enhanced excitation energy transfer under strong light-matter coupling: Insights from multi-scale molecular dynamics simulations, arXiv:2209.07309.
[38] D. Xu, A. Mandal, J. M. Baxter, S. W. Cheng, I. Lee, H. Su, S. Liu, D. R. Reichman, and M. Delor, Ultrafast imaging of coherent polariton propagation and interactions, arXiv:2205.01176.
[39] A. M. Alvertis, R. Pandya, C. Quarti, L. Legrand, T. Barisien, B. Monserrat, A. J. Musser, A. Rao, A. W. Chin, and D. Beljonne, First principles modeling of exciton-polaritons in polydiacetylene chains, J. Chem. Phys. **153**, 084103 (2020).
[40] P. W. Anderson, Absence of diffusion in certain random lattices, Phys. Rev. **109**, 1492 (1958).
[41] E. Abrahams, P. W. Anderson, D. C. Licciardello, and T. V. Ramakrishnan, Scaling Theory of Localization: Absence of Quantum Diffusion in Two Dimensions, Phys. Rev. Lett. **42**, 673 (1979).
[42] Y. Wang, X. Xia, L. Zhang, H. Yao, S. Chen, J. You, Q. Zhou, and X.-J. Liu, One-Dimensional Quasiperiodic Mosaic Lattice with Exact Mobility Edges, Phys. Rev. Lett. **125**, 196604 (2020).
[43] J. Cao and R. J. Silbey, Optimization of exciton trapping in energy transfer processes, J. Phys. Chem. A **113**, 13825 (2009).
[44] C. Chuang, C. K. Lee, J. M. Moix, J. Knoester, and J. Cao, Quantum Diffusion on Molecular Tubes: Universal Scaling of the 1D to 2D Transition, Phys. Rev. Lett. **116**, 196803 (2016).
[45] See Supplemental Material at http://link.aps.org/supplemental/10.1103/PhysRevLett.130.213602 for more information about the solution of the TC model and the numerical calculations.
[46] G. Engelhardt, G. Schaller, and T. Brandes, Bosonic Josephson effect in the Fano-Anderson model, Phys. Rev. A **94**, 013608 (2016).
[47] G. E. Topp, G. Schaller, and T. Brandes, Steady-state thermodynamics of non-interacting transport beyond weak coupling, Europhys. Lett. **110**, 67003 (2015).
[48] M. Fleischhauer, A. Imamoglu, and J. P. Marangos, Electromagnetically induced transparency: Optics in coherent media, Rev. Mod. Phys. **77**, 633 (2005).
[49] G. Engelhardt and J. Cao, Dynamical Symmetries and Symmetry-Protected Selection Rules in Periodically Driven Quantum Systems, Phys. Rev. Lett. **126**, 090601 (2021).
[50] F. Herrera and M. Litinskaya, Disordered ensembles of strongly coupled single-molecule plasmonic picocavities as nonlinear optical metamaterials, J. Chem. Phys. **156**, 114702 (2022).
[51] M. Reed and S. Barry, *Methods of Modern Mathematical Physics. II. Fourier Analysis, Self-Adjointness* (Academic Press, New-York-London, 1975), Section IX.3; Theorem IX.13.
[52] J. Wu, R. J. Silbey, and J. Cao, Generic Mechanism of Optimal Energy Transfer Efficiency: A Scaling Theory of the Mean First-Passage Time in Exciton Systems, Phys. Rev. Lett. **110**, 200402 (2013).
[53] C. K. Lee, J. Moix, and J. Cao, Coherent quantum transport in disordered systems: A unified polaron treatment of hopping and band-like transport, J. Chem. Phys. **142**, 164103 (2015).
[54] G. Engelhardt and J. Cao, Tuning the Aharonov-Bohm effect with dephasing in nonequilibrium transport, Phys. Rev. B **99**, 075436 (2019).
[55] A. Chenu and J. Cao, Construction of Multichromophoric Spectra from Monomer Data: Applications to Resonant Energy Transfer, Phys. Rev. Lett. **118**, 013001 (2017).
[56] R. Pandya, A. Ashoka, K. Georgiou, J. Sung, R. Jayaprakash, S. Renken, L. Gai, Z. Shen, A. Rao, and A. J. Musser, Tuning the coherent propagation of organic exciton-polaritons through dark state delocalization, Adv. Sci. **9**, 2105569 (2022).